The FASEB Journal

FASEB
Federation of American Societies for Experimental Biology

RESEARCH ARTICLE OPEN ACCESS

Pathogenic Gαo Mutants Drive Dominant GPCR Coupling in *GNAO1* Encephalopathies

Yonika A. Larasati[1] | Camille Rabesahala de Meritens[1] | Miriam Stoeber[2] | Vladimir L. Katanaev[1,3] | Gonzalo P. Solis[1]

[1]Translational Research Center in Oncohaematology, Department of Cell Physiology and Metabolism, Faculty of Medicine, University of Geneva, Geneva, Switzerland | [2]Department of Cell Physiology and Metabolism, Faculty of Medicine, University of Geneva, Geneva, Switzerland | [3]Translational Oncology Research Center, Qatar Biomedical Research Institute (QBRI), College of Health and Life Sciences, Hamad Bin Khalifa University (HBKU), Qatar Foundation, Doha, Qatar

Correspondence: Vladimir L. Katanaev (vladimir.katanaev@unige.ch) | Gonzalo P. Solis (gonzalo.solis@unige.ch)

Received: 6 September 2025 | **Revised:** 2 December 2025 | **Accepted:** 17 December 2025

Keywords: bimolecular fluorescence complementation (BiFC) | dystonia | epilepsy | G protein-coupled receptors (GPCRs) | GNAO1 | Gαo | heterotrimeric G proteins | movement disorders | neurodevelopmental disorders

ABSTRACT

Heterozygous mutations in *GNAO1*, which encodes the Gαo subunit of heterotrimeric G proteins, cause a spectrum of neurodevelopmental disorders ranging from early-onset epileptic encephalopathy to dystonia. Although the mechanisms underlying disease dominance remain incompletely understood, some functional disruptions in Gαo mutants have been described. Intriguingly, several Gαo variants have been independently reported to dominantly engage G protein-coupled receptors (GPCRs) or to sequester Gβγ—two seemingly incompatible mechanisms inferred from distinct, indirect biosensor assays. To clarify this apparent contradiction, we developed a split-YFP-based bimolecular fluorescence complementation (BiFC) assay to directly visualize receptor-G_o protein complexes at the plasma membrane. Using this system, we found that severe Gαo variants fail to disengage from activated Gi/o-coupled GPCRs, thereby preventing downstream receptor phosphorylation and endocytosis. By contrast, milder dystonia-linked mutants showed near-normal receptor internalization and only minor phosphorylation defects. These findings establish dominant GPCR coupling as a molecular hallmark of severe *GNAO1* encephalopathies and point to split-YFP BiFC as a robust platform for probing mutant G protein behavior in genetic disease.

1 | Introduction

G protein-coupled receptors (GPCRs) represent the largest and most diverse family of membrane receptors in metazoans [1, 2]. From neurotransmission and hormonal signaling to sensory perception and immune responses, GPCRs are essential for proper animal development and physiology [3, 4]. Signal transduction by GPCRs is mediated by heterotrimeric G proteins, composed of three subunits: α, β, and γ, with the Gα subunit conferring receptor specificity [5, 6]. In the inactive state, Gα is bound to GDP and associates tightly with the Gβγ dimer. Upon ligand binding, the GPCR undergoes a conformational change that catalyzes the exchange of GDP for GTP on Gα. This process activates the heterotrimeric G protein, causing Gα-GTP and Gβγ to dissociate and signal independently to downstream effectors. The signal is terminated when Gα hydrolyzes GTP to GDP through its intrinsic GTPase activity and associates with Gβγ, reforming the heterotrimer [7, 8]. Given their central role in GPCR signaling, it is perhaps unsurprising that mutations affecting heterotrimeric G protein subunits have been implicated in a variety of human diseases.

Historically, gain-of-function mutations in genes encoding Gα subunits have drawn most of the attention due to their

role as drivers in various cancers [9, 10]. These mutations produce constitutively active Gα proteins, resulting in persistent stimulation of oncogenic signaling pathways. More recently, however, a growing number of rare genetic disorders have been attributed to alternative mutations in Gα subunits [11, 12]. Among these, mutations in *GNAO1*, the gene encoding for Gαo, have been implicated in a broad spectrum of neurodevelopmental disorders [13–15]. The most severe conditions were originally classified as Developmental and Epileptic Encephalopathy 17 (DEE17; OMIM #615473) and Neurodevelopmental Disorder with Involuntary Movements (NEDIM; OMIM #617493) [16, 17]. In recent years, *GNAO1* mutations have also been associated with milder conditions, including autism and intellectual disability, parkinsonism, and dystonia [18–20]. More than 250 patients have been reported worldwide, the vast majority carrying missense mutations, with only a few cases of deletions, frameshifts, duplications, short indels, and splice-site mutations described [15]. Treatment responses among *GNAO1* patients are highly variable and typically poor, particularly in cases involving epilepsy and/or movement disorders. This underscores the urgent need for more effective therapies for these severe conditions.

At the molecular level, Gαo mutants associated with severe phenotypes display a set of interconnected pathogenic mechanisms, including severely impaired guanine nucleotide handling, misfolding in the GTP-bound active state, and neomorphic binding to Ric8A/B chaperones, all of which converge to perturb the broader GPCR signaling network [21–26]. By contrast, variants on the milder end of the *GNAO1*-related disorder spectrum exhibited only mild biochemical defects, with some mutants lacking the neomorphic property entirely, while others retained trapping of Ric8A but not Ric8B [19, 20, 23, 27]. Furthermore, the most severe DEE17 Gαo variants tend to lose plasma membrane (PM) localization and Gβγ binding, whereas mutants linked to NEDIM or milder phenotypes retain near-normal association with both PM and Gβγ [21–23].

Another emerging feature of several pathogenic *GNAO1* mutations is their apparent dominant coupling to GPCRs. A study using a bioluminescence resonance energy transfer (BRET)-based assay to measure free Gβγ during GPCR stimulation showed that clinically severe Gαo variants partially inhibit activation of the wild-type protein, acting in a dominant-negative (DN) manner [21]. These Gαo mutants displayed poor disengagement from Gβγ despite normal (or even enhanced) coupling to activated GPCRs—the latter determined indirectly by a split-NanoLuc assay measuring Gβγ proximity to the receptor. Based on this, the authors proposed that the DN effect arises from nonproductive interactions between the mutant Gαo and GPCRs. Along the same lines, we found that many clinically severe Gαo mutants exhibit normal or even enhanced GPCR coupling despite poor binding to Gβγ, using a different BRET-based assay that directly monitors GPCR engagement by Gα [23]. This dominant coupling mechanism was recently confirmed for the epileptic Gαo K46E variant, which forms a nonproductive complex with both Gβγ and the activated GPCR, as revealed by cryo-electron microscopy [28]. By contrast, an earlier study using yet another BRET-based assay that directly measures Gβγ disengagement from Gα described an alternative DN mechanism for some of the same Gαo mutants: sequestration of Gβγ, due to impaired adoption of the active conformation required for their dissociation, without sequestering the GPCR [22].

Thus, dominant GPCR coupling by pathogenic Gαo mutants can currently only be inferred using a combination of optical biosensors, leading to apparent mechanistic contradictions. To resolve this, we developed a novel assay to directly visualize the dominant GPCR coupling behavior of Gαo variants. We employed bimolecular fluorescence complementation (BiFC), a method based on the structural reassembly of two non-fluorescent N- and C-terminal fragments of a fluorescent protein into a functional fluorophore when both fragments are in close proximity [29]. Using the split-YFP-based BiFC approach, we show that *GNAO1* mutations associated with the most severe phenotypes result in dominant GPCR coupling by the mutant Gαo, likely caused by a defective receptor-Gα uncoupling.

2 | Material and Methods

2.1 | Antibodies and Reagents

Primary antibodies (Abs) for immunofluorescence (IF) and Western blots (WBs): monoclonal Abs (mAbs) anti-Gαo (clone A2, sc-13 532, RRID:AB_2111645; IF: 1/50) and anti-Gαo (clone E1, sc-393 874, RRID:AB_2941093; WB: 1/250) were from Santa Cruz Biotechnology (Dallas, TX, USA); mAb anti-HA-tag (clone 3F10, 11 867 423 001, RRID:AB_390918; IF: 1/500) was from Roche (Basel, Switzerland). Polyclonal antibodies (pAbs) anti-M_2R (7TM0014N; WB: 1/1000) and anti-pT307/pS309 (7TM0014D; IF: 1/500, WB: 1/1000) were from 7TM Antibodies (Jena, Thuringia, Germany); pAbs anti-GFP (PABG1, RRID:AB_2749857; IF: 1/1000) and anti-GFP (50430–2-AP, RRID:AB_11042881; WB: 1/5000) were from Proteintech (Rosemont, IL, USA).

All secondary Abs for immunofluorescence (IF) and Western blots (WBs) were from Jackson ImmunoResearch (West Grove, PA, USA): anti-Mouse Cy5-conjugated (715–175-151, RRID:AB_2340820; IF: 1/500), anti-Rabbit Cy3-conjugated (711–165-152, RRID:AB_2307443; IF: 1/500), anti-Rat Cy3-conjugated (112–165-143, RRID:AB_2338250; IF: 1/500), anti-mouse HRP-conjugated (115–035-146, RRID:AB_2307392; WB: 1/5000), and anti-rabbit HRP-conjugated (111–035-144, RRID:AB_2307391; WB: 1/5000).

Acetylcholine (A2661), isoproterenol (I6504), and DAPI (32670) were from Sigma-Aldrich (Burlington, MA, USA), and EGF-Rhodamine (E3481) was from Thermo Fisher Scientific (Waltham, MA, USA). Fentanyl (CAS no. 1443-54-5) was obtained from the University Hospital of Geneva with Département de la sécurité, de la population et de la santé (DSPS) authorization from the Canton of Geneva.

2.2 | Plasmids and Molecular Cloning

Plasmids encoding for the untagged Gαo wild-type and pathogenic mutants were published earlier [23, 27, 30]. Untagged Gαo ins4A was kindly provided by Nevin A. Lambert (Augusta

University, GA, USA). To generate the mRFP internal tagging of Gαo (at Gly92; Gαo-mRFP), the mRFP sequence was amplified by PCR from pmRFP-C1 [30] using the oligonucleotide primers For: 5′–GTCGCCGGGCCCGCCTCCTCCGAGGAC–3′ and Rev: 5′–TTTAAAGCAAGTAAAACCTC–3′. The PCR product was cloned in-frame into the PspOMI/BsrGI sites of Gαo-GFP [31]. The sequences for the split-YFP fragments YN (aa 1–158) and YC (aa 159–239) containing a flexible 10-amino acid (GGGGSGGGGS) linker were kindly provided by Daniel F. Legler (Institute of Cell Biology and Immunology Thurgau, Switzerland). To produce the Gαo-YC constructs (internal YC insertion at Gly92), the YC sequence was amplified by PCR using the primers For: 5′–GGATCCACCGGTCCTC ACCGGGCCCGGTGGCGGTGGCTCTGG–3′ and Rev: 5′–AGATCTGAGTCCGGACTTGTACACGGACCC–3′. The resulting product was cloned in-frame into the PspOMI/BsrGI sites of Gαo-GFP wild-type and mutants [23, 27]. The Gαo-YC for ins4A was obtained by replacing the AgeI/PspOMI fragment in Gαo-YC wild-type with the AgeI/NotI fragment from untagged Gαo ins4A. The GFP-M_2R construct was generated by cloning in-frame the fragment blunted-EcoRI/XhoI from the untagged M_2R plasmid (MAR0200000; cDNA Resource Center, Bloomsburg, PA, USA) into the Eco53KI/SalI sites of the PrP-leader-GFP plasmid [32]. To produce the M_2R-YN construct, we first PCR amplified the YN sequence with the primers For: 5′–AGCCCGGACC GGTCCTCACCATGGATGGTGGCGGTGGCTC–3′ and Rev: 5′–TTTAGGTGGCGGCCGCGAATAGGACCCTCTAGATTAC–3′. The PCR product was digested with AgeI/NotI and ligated in-frame into the AgeI/NotI sites of M_2R-NLuc [23]. The sequence for a signal peptide-HA tag was generated by the primers For: 5′–TCGACCACCATGAAGACGATCA TCGCCCTGAGCTACATCTTCTGCCTGGTATTCGCCT ACCCATACGATGTTCCTGACTATGCGG–3′ and Rev: 5′–A ATT CCG CAT AGT CAG GAA CAT CGT ATG GGT AGG CGA ATA CCA GGC AGA AGA TGT AGC TCA GGG CGATGATCGTCTTCATGGTGG–3′ and cloned in-frame into the XhoI/EcoRI sites upstream of the M_2R. For the M_2R-YC plasmid, the YC fragment was amplified by PCR using the primers For: 5′–ACTATGAACCGGTACT CACCATGGATGGTGGCGGTGGCTC–3′ and Rev: 5′–GCAACTAGAAGGCACAGTCGAGG–3′, and cloned in-frame into the AgeI/NotI sites of the final M_2R-YN. The β_2AR-YN plasmid was obtained by cutting the NheI/AgeI coding fragment from β_2AR-mCFP (plasmid 38260; Addgene, Watertown, MA, USA) and insertion into the same sites of M_2R-YN. The MOR-YN construct was produced by cutting the XhoI/XmaI coding sequence from the MOR-GFP plasmid [33], and ligation into the XhoI/AgeI sites of M_2R-YN. The T2A-based bicistronic Gβ3-YN-Gγ3 construct—referred to as YN-Gγ3 for simplicity—was generated through a two-step cloning. First, the single YN-Gγ3 plasmid was cloned by PCR amplification of the YN sequence using the primers For: 5′–CTATAGGACC GGTCAAGACCATGGTGAGCAAGGGCGAGGA–3′ and Rev: 5′–TGCTCGAGTGTACACGGACCCACCACCTCCAGAGC–3′, and the YN fragment was cloned in-frame into the AgeI/BsrGI sites of GFP-Gγ3 [30]. Then, a T2A-based bicistronic Gβ3-cpVenus-Gγ9 plasmid was created by cutting the NheI/SalI insert from Go1-CASE [34] (provided by Gunnar Schulte; Karolinska Institutet, Sweden) and ligation of the fragment into the same sites of pEGFP-C1 (Clontech, San Jose, CA, USA). The final YN-Gγ3 construct was generated by cutting the YN-Gγ3 coding sequence with AfeI/PspOMI, and ligation of this fragment into the blunted-AgeI/PspOMI of Gβ3-cpVenus-Gγ9. A T2A-based bicistronic untagged Gβ3-Gγ9 plasmid (referred to as Gβ3γ9) was generated by cutting out the cpVenus sequence from Gβ3-cpVenus-Gγ9 with AgeI/BspEI, and religation to produce an in-frame Gβ3-T2A-Gγ9 construct.

2.3 | Cell Lines and Culture Conditions

Human HEK293T (CRL-3216, RRID:CVCL_0063; ATCC, Manassas, VA, USA) cells were grown in DMEM, supplemented with 10% FCS, 2 mM L-glutamine, and 1% penicillin–streptomycin (all from Thermo Fisher Scientific, Waltham, MA, USA) at 37°C and 5% CO_2. All vector transfections were carried out with X-tremeGENE HP (XTGHP-RO; Roche, Basel, Switzerland) according to the manufacturer's instructions.

2.4 | Split-YFP-Based BiFC Assay and Microscopy

For the split-YFP assay between GPCRs and Gαo, HEK293T cells were co-transfected with GPCR-YN constructs (M_2R, MOR, or β_2AR), Gαo-YC (wild-type, pathogenic mutants, or the control ins4A), and Gβ3γ9 at a plasmid ratio of 2.5:2.5:1. For the split-YFP assay between M_2R and Gγ3, cells were co-transfected with M_2R-YC, YN-Gγ3, and untagged Gαo variants or empty plasmid at the same ratio. After 6 h, cells were trypsinized, seeded onto poly-L-lysine-coated coverslips, and cultured—or co-cultured in the case of the M_2R-Gγ3 split-YFP assay—for an additional 15 h in complete DMEM.

For endocytosis analysis of GPCR-YFP-Gαo complexes, cells were stimulated for 10, 20, and/or 30 min with 100 μM acetylcholine (ACh) for M_2R, 1 μM fentanyl for MOR, or 10 μM isoproterenol for β_2AR. To determine M_2R phosphorylation, cells were stimulated with 100 μM ACh for 7 min. To evaluate EGF uptake, cells were treated with 10 ng/mL EGF-Rhodamine for 10 min as previously described [35].

After treatments, cells were fixed with 4% PFA in PBS for 20 min and permeabilized with ice-cold 0.1% Triton X-100 in PBS for 1 min—this step was omitted under non-permeabilizing conditions. Cells were then blocked for 1 h in PBS supplemented with 1% BSA (810 533; Millipore, Burlington, MA, USA), incubated with primary antibodies in blocking buffer for 2 h at room temperature (RT), washed, and subsequently incubated with fluorescently labeled secondary antibodies and DAPI in blocking buffer for 2 h at RT. Coverslips were mounted with VECTASHIELD (H-1700; Vector Laboratories, Newark, CA, USA) on microscope slides. For immunostaining against phosphorylated M_2R, all steps were performed in TBS instead of PBS.

Samples were recorded using a Plan-Apochromat 63×/1.4 oil objective on an LSM800 confocal microscope with ZEN 3.7 software (all from Zeiss, Oberkochen, Baden-Württemberg, Germany). When quantification was required, all images were acquired using identical confocal settings across all channels. Mean fluorescence intensities, cell area, and vesicle-like structure counts were determined from confocal images either manually or semi-automatically using in-house scripts, all

with ImageJ v1.54p (RRID:SCR_002285; National Institutes of Health).

2.5 | PM Targeting of GFP-M_2R

HEK293T cells were co-transfected with GFP-M_2R, untagged Gαo variants (wild-type, pathogenic mutants, or the control ins4A), and Gβ3γ9 at a plasmid ratio of 2.5:2.5:1. Samples were immunostained under non-permeabilizing conditions, and image acquisition and quantification were performed as described above.

2.6 | Immunoprecipitation

The recombinant GST-tagged nanobody against GFP was expressed in *Escherichia coli* Rosettagami (71 351; Novagen, Madison, WI, USA) and purified using Glutathione Sepharose 4B beads according to the manufacturer's instructions. Protein purity was confirmed by SDS-PAGE and Coomassie blue staining.

HEK293T cells were co-transfected with the split-YFP constructs for M_2R, Gαo, and Gβ3γ9, or with GFP-M_2R, untagged Gαo variants, and Gβ3γ9, using the same plasmid ratio described above. After 24 h of transfection, cells were stimulated with 100 μM ACh for 5 min, then immediately resuspended in ice-cold TBS-lysis buffer (20 mM Tris–HCl, pH 7.5, 150 mM NaCl, 1% Triton X-100, 10% glycerol) supplemented with protease (04693132001) and phosphatase (04906837001) inhibitor cocktails from Roche (Basel, Switzerland). Lysates were passed 15 times through a 25-G needle and cleared by centrifugation at 15000xg for 15 min at 4°C. Supernatants were incubated with 2 μg of purified anti-GFP nanobody for 30 min on ice, followed by addition of 20 μL of Glutathione Sepharose 4B beads (17 075 601; Cytiva, Marlborough, MA, USA) and rotation for 3 h at 4°C.

Beads were washed repeatedly with TBS-lysis buffer and resuspended in Laemmli sample buffer. Inputs and beads were heated at 50°C for 30 min and analyzed by SDS-PAGE Western blotting using Abs against phospho-M_2R (pT307/pS309), total M_2R, Gαo, and GFP. HRP-conjugated secondary antibodies were used for detection, with all antibody incubations performed in TBS containing 1% BSA. Signal was visualized using enhanced chemiluminescence (ECL) on a Fusion FX6 Edge system (Vilber). Quantification of all WBs was performed using ImageJ v1.54p. Final image preparation was done in EvolutionCapt v18.11 (RRID:SCR_023580; Vilber, Collégien, Île-de-France, France) and CorelDRAW 2020 (RRID:SCR_014235; Corel Corporation, Ottawa, ON, Canada).

2.7 | Statistics

Data were analyzed using GraphPad Prism (version 10.5.0; GraphPad Software, San Diego, CA, USA). Box-and-whisker plots indicate the median (middle line), the 25th and 75th percentiles (box), and the lowest and highest values (whiskers). Bar plots represent mean ± SEM. Multiple comparisons were assessed by one-way ANOVA followed by Dunnett's or Šídák's multiple comparisons tests, as indicated. A P value < 0.05 was considered statistically significant. All P values are reported in the figures and legends.

3 | Results

3.1 | Dominant GPCR Coupling by Pathogenic Gαo Mutants Blocks Receptor Endocytosis

To determine whether pathogenic Gαo mutants indeed engage in dominant coupling with GPCRs, we sought to develop a single assay capable of visualizing this process. However, microscopic visualization of plasma membrane (PM)-localized GPCRs can be challenging, as exogenous expression often leads to their accumulation in the endoplasmic reticulum and Golgi apparatus due to saturation of the cellular folding and trafficking machinery [36]. Consistent with this, expression of an N-terminal GFP fusion of the M_2 muscarinic acetylcholine receptor (GFP-M_2R) in HEK293T cells results in prominent intracellular retention (Figure S1A). We selected M_2R for this study because it is a prototypical Gi/o-coupled GPCR [37] and because we previously observed that severe Gαo mutants exhibit enhanced coupling to this receptor [23], consistent with dominant GPCR engagement.

To overcome this limitation, we employed a split-YFP-based BiFC assay (hereafter split-YFP), previously used to visualize the PM interaction between the chemokine GPCR CCR7 and the Src tyrosine kinase [38]. Like Src, Gα subunits associate with the membrane via lipid modifications [39, 40], which target Gαo to the PM and Golgi in HEK293T cells (Figure S1B) [30]. Based on these observations, we reasoned that a split-YFP assay combining M_2R and Gαo would enable selective visualization of the PM-localized receptor pool. We further speculated that the irreversible nature of the split-YFP complementation would bias M_2R toward coupling with Gαo over endogenous Gα subunits, thereby enhancing both the specificity and sensitivity of the assay.

We first generated M_2R and Gαo constructs carrying each of the YFP fragments—N-terminal (YN) or C-terminal (YC)—fusing them to the intracellular C-terminus of the receptor and internally at Gly92 in Gαo (Figure 1A). One of the two possible combinations—M_2R-YN and Gαo-YC (M_2R-YFP-Gαo; Figure 1B) – produced a much stronger fluorescence signal than the opposite configuration (not shown), confirming that the orientation of the YFP halves is critical for efficient complementation [41]. As speculated, the M_2R-YFP-Gαo complex was strongly visualized at the PM of HEK293T cells, with only a few intracellular structures visible (Figure 1B). Notably, acetylcholine (ACh) stimulation for 10 min led to the prominent appearance of vesicles/endosomes and a marked reduction in PM signal, suggesting endocytosis of the M_2R-YFP-Gαo complex (Figure 1C). Although Gαo typically remains at PM following GPCR stimulation [30, 42], the irreversibility of split-YFP complementation likely drives its co-internalization with the receptor [29].

Next, we performed the split-YFP assay for M_2R and several pathogenic Gαo mutants. We selected three of the most recurrent

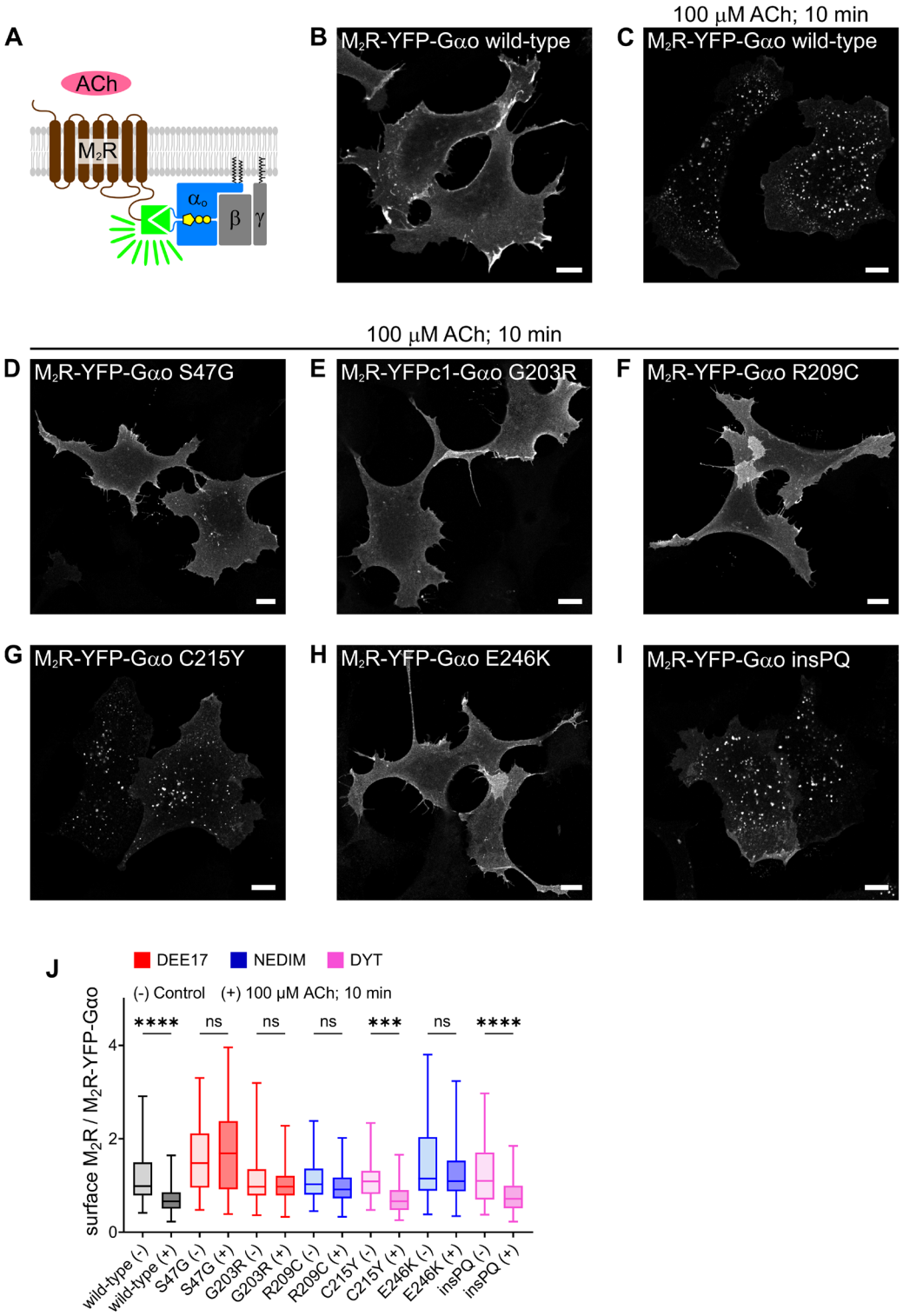

FIGURE 1 | Clinically severe Gαo mutants disrupt M_2R endocytosis. (A) Illustration of the split-YFP assay applied to M_2R and heterotrimeric Gαoβγ. (B,C) Representative confocal images of HEK293T cells expressing the M_2R-YFP-Gαo complex at steady state (B) and after 10 min of acetylcholine (ACh) stimulation (C). (D-I) Confocal images of ACh-stimulated HEK293T cells expressing the M_2R-YFP-Gαo complex containing the Gαo mutants S47G (D), G203R (E), R209C (F), C215Y (G), E246K (H), and insPQ (I). Scale bars, 10 μm. (J) Quantification of ACh-mediated M_2R internalization, expressed as the surface level of M_2R normalized to total M_2R-YFP-Gαo signal. Gαo mutant associations with DEE17, NEDIM and DYT phenotypes are color-coded. Box plots indicate the median (middle line), the 25th and 75th percentiles (box), and the lowest and highest values (whiskers); two-three independent experiments (wild-type, $n = 78$; wild-type +ACh, $n = 85$; S47G, $n = 55$; S47G + ACh, $n = 51$; G203R, $n = 59$; G203R + ACh, $n = 69$; R209C, $n = 78$; R209C + ACh, $n = 76$; C215Y, $n = 59$; C215Y + ACh, $n = 74$; E246K, $n = 63$; E264K + ACh, $n = 65$; insPQ, $n = 54$; insPQ + ACh, $n = 63$). Statistical analysis was performed using one-way ANOVA followed by Šídák's multiple comparisons test; ***$p < 0.001$, ****$p < 0.0001$, and ns: Not significant.

Gαo variants—G203R, R209C, and E246K—that may act as DN, either through nonproductive GPCR coupling [21, 23] or via Gβγ sequestration [22]. We also included the S47G mutant, which shows normal to high GPCR coupling but poor Gβγ dissociation [21, 23], and has alternatively been described as non-functional [22]. Among these, Gαo S47G and G203R are associated with the most severe DEE17 phenotype, while R209C and E246K are linked to NEDIM. Two Gαo mutants associated with a milder dystonia (DYT) phenotype were also analyzed: C215Y and the recurrent splice-site variant c.724-8G > A, which results in an in-frame insertion of two additional residues (Pro-Gln) at position T241 (T241_N242insPQ; hereafter insPQ) [18, 23, 27].

As shown in Figure 1, split-YFP complementation was achieved for all pathogenic Gαo mutants. However, ACh stimulation revealed striking differences, with DEE17 and NEDIM variants strongly impairing internalization of the M_2R-YFP-Gαo complex and DYT mutants showing no apparent defects (Figure 1D–I). With longer ACh stimulation, the wild-type M_2R-YFP-Gαo complex accumulated on larger endosomes at 20 and 30 min (Figure S2A,B), structures resembling early/late endosomes [43]. In contrast, complexes formed by the DEE17 and NEDIM variants largely remained at the PM even after 30 min, indicating that ACh-induced M_2R internalization is blocked rather than merely delayed by the severe Gαo mutants (Figure S2D–I).

To quantify endocytosis, we analyzed the PM localization of M_2R-YN before and after ACh stimulation using immunostaining—under non-permeabilizing conditions—against an extracellular HA-epitope at the N-terminus of the construct (Figure S3A–G). The extracellular HA-signal was normalized to the intrinsic fluorescence of the M_2R-YFP-Gαo complex to account for variability in expression levels across cell populations. As expected, a significant reduction of the relative PM pool of M_2R was observed only for wild-type Gαo and the mild DYT variants C215Y and insPQ (Figure 1J). For these Gαo mutants, we noticed that the HA-derived M_2R signal was strongly reduced upon ACh stimulation in some cells, but not in others—particularly those with higher expression levels (Figure S3A–G). This variability may reflect saturation of the receptor endocytic pathway due to overexpression [44].

We also noticed that the overall YFP signal in cells expressing M_2R-YFP-Gαo complexes was reduced for some of the pathogenic variants compared to wild-type. Quantification revealed that the DEE17 S47G, NEDIM E246K, and DYT insPQ variants formed significantly lower levels of M_2R-YFP-Gαo complexes (Figure S3H). This is likely the outcome of reduced expression of the corresponding Gαo-YC constructs (Figure S3I,J), consistent with the known tendency of many pathogenic Gαo mutants to express at lower levels [22, 23]. These expression differences, however, do not account for the defective internalization observed for DEE17 and NEDIM variants, as the DYT insPQ variant—despite a similar reduction in M_2R-YFP-Gαo formation—underwent robust internalization.

The most straightforward explanation for the failure of M_2R-YFP-Gαo complexes formed by DEE17/NEDIM variants to undergo endocytosis is a defect in receptor-Gαo uncoupling, which prevents progression toward receptor internalization. However, we cannot exclude the possibility that these severe Gαo mutants may impair endocytosis more broadly. To address this, we examined the internalization of an unrelated receptor, epidermal growth factor receptor (EGFR), using fluorescently labeled EGF-Rhodamine as readout [35]. EGF-Rhodamine uptake in HEK293T cells expressing the M_2R-YFP-Gαo complex was comparable to that in non-transfected neighboring cells (Figure S4A–G). Furthermore, quantification of internalized EGF-Rhodamine in cells expressing M_2R-YFP-Gαo revealed no significant differences among the various Gαo variants (Figure S4H). These results suggest that expression of DEE17/NEDIM Gαo mutants does not broadly interfere with receptor endocytosis.

Next, we tested the specificity of the split-YFP assay using different GPCRs. We selected the μ-opioid receptor (MOR; Figure S5A), which is known to engage Gαo, and the β_2-adrenoceptor (β_2AR; Figure S6A), which signals primarily through Gαs [45, 46]. Notably, split-YFP complementation was effectively achieved between wild-type Gαo-YC and either MOR-YN or β_2AR-YN, with MOR-YFP-Gαo (Figure S5B) and β_2AR-YFP-Gαo (Figure S6B) complexes localized primarily at the PM of HEK293T cells. These results indicate that split-YFP complementation with Gαo is not selective for Gi/o-coupled receptors. Recapitulating the pattern observed with M_2R, stimulation with fentanyl for 10 min induced internalization of the wild-type MOR-YFP-Gαo complex into vesicles/endosomes (Figure S5C), a pattern also observed for the DYT variants, but not for the mutants associated with DEE17/NEDIM (Figure S5D–I). Conversely, isoproterenol treatment induced the endocytosis of the β_2AR-YFP-Gαo complex formed by the wild-type protein and all pathogenic variants alike (Figure S6C–I), suggesting that the dominant GPCR coupling of Gαo mutants is specific for Gi/o-coupled receptors. This finding further implies that split-YFP complementation between β_2AR and Gαo does not block the ability of the receptor to couple with endogenous G proteins.

3.2 | ACh-Mediated M_2R Phosphorylation Is Blocked by Dominant Gαo Variants in the Split-YFP Assay

Following the dissociation of G proteins from activated GPCRs, a cascade of molecular events is initiated. GPCR kinases (GRKs) are recruited to the receptors, where they bind to the same intracellular pocket previously occupied by the Gα subunit [47]. GRK recruitment enables phosphorylation of multiple residues within the intracellular loops and/or C-terminus of the GPCR. This promotes the subsequent recruitment of β-arrestins, which act as scaffolds for the clathrin-mediated endocytic machinery, ultimately driving receptor internalization [48].

Our findings support the notion that the most severe pathogenic Gαo variants fail to disengage from activated GPCRs, remaining dominantly coupled and thereby preventing GRK recruitment and subsequent receptor phosphorylation. To test this prediction, we analyzed M_2R phosphorylation using the split-YFP assay. We used a non-pathogenic Gαo construct carrying a four-alanine insertion in the C-terminal α5-helix (ins4A) as control,

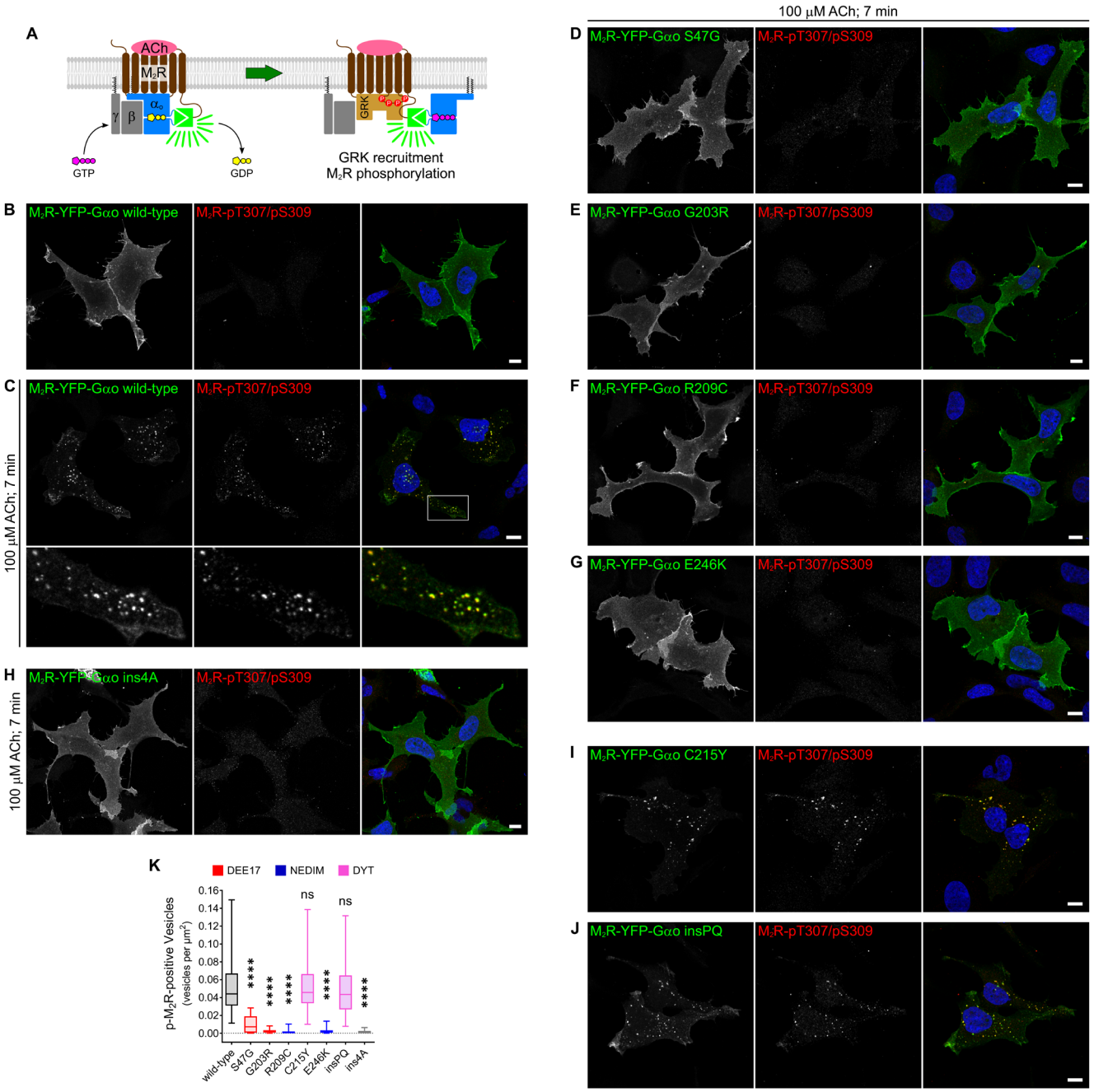

FIGURE 2 | Inhibition of ACh-mediated phosphorylation of M_2R by pathogenic Gαo variants. (A) Schematic representation of the molecular events following ACh stimulation that lead to M_2R phosphorylation, as illustrated using the split-YFP assay. (B,C) Representative confocal images of HEK293T cells expressing the M_2R-YFP-Gαo complex at steady state (B) and after 7 min of acetylcholine (ACh) stimulation (C). Cells were immunostained with a specific antibody recognizing dual phosphorylation at T307 and S309 of M_2R (M_2R-pT307/pS309), and counterstained with DAPI to visualize nuclei. A boxed region in (C) is shown at higher magnification in the lower panels. (D-H) ACh-stimulated HEK293T cells expressing the M_2R-YFP-Gαo complex with the Gαo mutants S47G (D), G203R (E), R209C (F), E246K (G), C215Y (I), insPQ (J), and the control ins4A (H). Cells were prepared as in (C). Scale bars, 10 µm. (K) Quantification of ACh-mediated endocytic events, expressed as the number of vesicle-like structures positive for both M_2R-YFP-Gαo and anti-pT307/pS309 staining, normalized to cell area. Associations of Gαo mutants with DEE17, NEDIM, and DYT phenotypes are color-coded. Box plots indicate the median (middle line), the 25th and 75th percentiles (box), and the lowest and highest values (whiskers); two-three independent experiments (wild-type, $n = 46$; S47G, $n = 43$; G203R, $n = 46$; R209C, $n = 44$; C215Y, $n = 48$; E246K, $n = 47$; insPQ, $n = 50$; ins4A, $n = 46$). Statistical analysis was performed using one-way ANOVA followed by Dunnett's multiple comparisons test; ****$p < 0.0001$ and ns: Not significant.

which is known to abolish G protein release from activated receptors [49, 50]. As expected, Gαo ins4A prevented ligand-mediated internalization of both M_2R Figure S7A–C and MOR Figure S7D–F in the split-YFP assay.

GRK-mediated phosphorylation of M_2R targets several Ser/Thr residues in the third intracellular loop (Figure 2A) [51]. We immunostained HEK293T cells expressing the M_2R-YFP-Gαo complex using a specific antibody that recognizes dual

phosphorylation at Thr307 and Ser309 (pT307/pS309). In unstimulated cells, the anti-pT307/pS309 signal was minimal in both transfected and non-transfected cells (Figure 2B). However, following 7 min of ACh stimulation, robust anti-pT307/pS309 staining appeared and closely colocalized with endocytic M_2R-YFP-Gαo–positive vesicles (Figure 2C). Neighboring untransfected cells showed no increase in the pT307/pS309 signal after stimulation, consistent with the absence of endogenous M_2R expression in the parental HEK293 line [52].

Notably, the Gαo variants associated with the severe DEE17/NEDIM phenotypes exhibited weak pT307/pS309 staining following ACh stimulation (Figure 2D–G). Since the ins4A construct produced an equivalent effect (Figure 2H), this result supports the notion that Gαo mutants dominantly couple to M_2R, thereby preventing GRK recruitment. In contrast, the DYT-associated mutants retained robust phospho-M_2R staining, similar to wild-type Gαo (Figure 2I,J). To quantify endocytic events, we counted the number of vesicle-like structures positive for both M_2R-YFP-Gαo and pT307/pS309 and normalized to the cell area (Figure 2K). A marked reduction in phospho-M_2R-YFP-Gαo–positive vesicles was observed for the DEE17/NEDIM variants and ins4A, whereas DYT mutants exhibited values comparable to wild-type.

To confirm the defects in ACh-mediated M_2R phosphorylation, we took advantage of an anti-GFP nanobody [31] that enables specific immunoprecipitation (IP) of the reconstituted split-YFP, but not the individual YN and YC fragments (Figure S8). In Western blots following IPs, four distinct protein species can be detected using M2R- and Gαo-specific antibodies: the M_2R-YN and Gαo-YC monomers, a monomeric M_2R-YFP-Gαo complex, and a higher molecular weight species, possibly corresponding to a M_2R-YFP-Gαo dimer (Figure S8). This likely reflects the known tendency of M_2R to form dimers and higher-order oligomers [53].

Corroborating the cell imaging data, IP of split-YFP complexes containing wild-type Gαo showed no detectable anti-pT307/pS309 signal for M_2R at steady state, whereas strong signals emerged following 5 min of ACh stimulation in three species: M_2R-YN, the monomeric, and the dimeric forms of the M_2R-YFP-Gαo complex (Figure 3A). In contrast, M_2R-YFP-Gαo complexes formed by the most severe DEE17/NEDIM mutants exhibited a marked reduction in anti-pT307/pS309 reactivity. Unexpectedly, both DYT-associated Gαo variants showed a modest reduction in M_2R phosphorylation. Quantification revealed a 60%–85% reduction for the DEE17/NEDIM variants, and over 90% for Gαo ins4A (Figure 3B). DYT mutants, on the other hand, showed a significant but smaller 20%–25% decrease, suggesting that these variants partially impair GRK recruitment—although not to a degree that prevents receptor endocytosis.

3.3 | Untagged Gαo Mutants Recapitulate M_2R Endocytosis and Phosphorylation Defects

While the split-YFP assay provides a powerful tool to visualize these interactions, it relies on internally tagged Gαo constructs, which could theoretically introduce artifacts not present in native, untagged proteins. To address this, we next tested whether the observed effects also occur with untagged Gαo variants.

We first employed the split-YFP assay for M_2R and Gγ3 (Figure 4A), and found that the combination of M_2R-YC and YN-Gγ3 produced a much stronger fluorescence signal than the reverse configuration (not shown). To test dominant GPCR coupling and receptor endocytosis, we expressed different construct sets in two separate HEK293T cell populations—M_2R-YC and YN-Gγ3 with or without untagged Gαo—and then co-cultured them. After 7 min of ACh treatment, cells were immunostained for Gαo and pT307/pS309. Anti-Gαo signal was absent in non-transfected HEK293T cells, consistent with the lack of Gαo expression in the parental HEK293 line [52]. ACh stimulation triggered robust internalization of the M_2R-YFP-Gγ3 complex in the presence or absence of wild-type Gαo expression, suggesting that endogenous Gα subunits were sufficient to engage the receptor (Figure 4B). Notably, co-expression of the DEE17/NEDIM variants markedly inhibited both M_2R phosphorylation and endocytosis, contrasting with the normal response observed in adjacent Gαo-negative cells (Figure 4C–F).

Finally, we moved beyond the split-YFP assay and analyzed ACh-mediated phosphorylation of GFP-M_2R upon co-expression of untagged Gαo variants (Figure 5A). We selected the GFP-M_2R construct because it lacks intracellular tags, thereby avoiding potential artifacts originating from the receptor. We first examined whether the PM localization of GFP-M_2R was affected by any Gαo variant. To this end, we immunostained the extracellular M_2R pool under non-permeabilizing conditions using an anti-GFP antibody and normalized the signal to the total GFP fluorescence to account for differences in expression (Figure S9A–H). Quantification showed that GFP-M_2R surface targeting was unaffected by co-expression of Gαo variants (Figure S9I).

As expected, IP analysis revealed no detectable phosphorylation of GFP-M_2R at steady state, whereas a strong anti-pT307/pS309 signal was observed following 5 min of ACh stimulation (Figure 5B). Remarkably, all pathogenic Gαo mutants reduced GFP-M_2R phosphorylation, following a pattern closely resembling that observed with the split-YFP assay. Quantification revealed a pronounced 65%–80% reduction in M_2R phosphorylation upon co-expression of the DEE17/NEDIM variants, and ~95% reduction for the Gαo ins4A mutant (Figure 5C). In contrast, co-expression of the DYT variants C215Y and insPQ led to more modest reductions of 20% and 30%, respectively.

Altogether, this study indicates that pathogenic Gαo variants remain persistently and dominantly coupled to activated GPCRs. These findings highlight a critical pathogenic mechanism in *GNAO1* encephalopathies and establish a robust split-YFP assay for its detection and potential therapeutic targeting.

4 | Discussion

Pathogenic *GNAO1* mutations disrupt multiple aspects of Gαo function [21–23]. Two distinct mechanisms—nonproductive

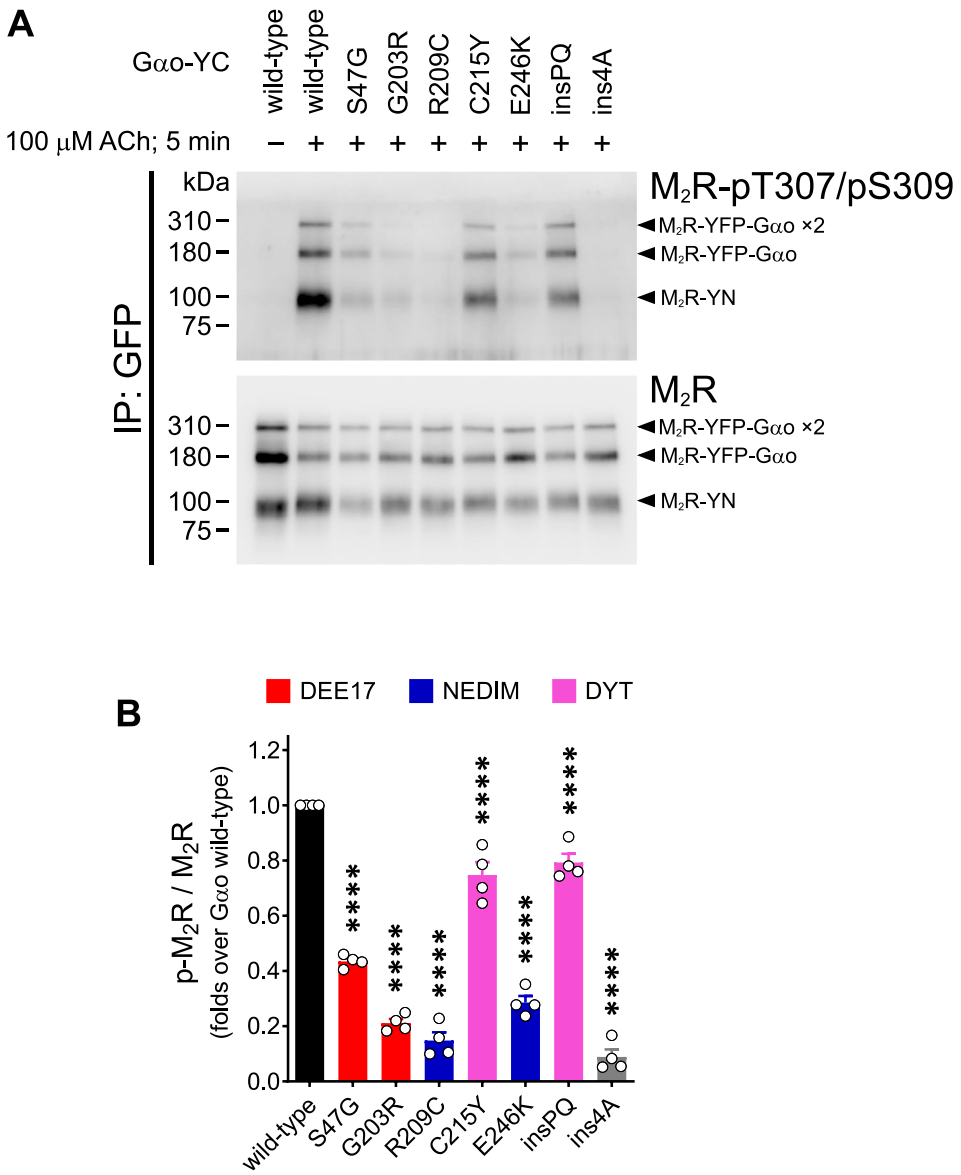

FIGURE 3 | Immunoprecipitation of the M_2R-YFP-Gαo complex confirms impaired recephosphorylation by pathogenic Gαo variants. (A) HEK293T cells expressing the split-YFP constructs M_2R-YN and Gαo-YC (wild-type, pathogenic mutants, and the ins4A control) were stimulated with 100 μM acetylcholine (ACh) for 5 min and subjected to immunoprecipitation (IP) using an anti-GFP nanobody. Western blotting and immunodetection were performed with antibodies against phosphorylated (pT307/pS309) and total M_2R. Arrowheads indicate M_2R-YN, and the monomeric and dimeric forms of the M_2R-YFP-Gαo complex. (B) Quantification of M_2R phosphorylation levels relative to total receptor ($n = 4$). Gαo mutant associations with DEE17, NEDIM, and DYT phenotypes are color-coded. Data represent mean ± SEM. Statistical analysis was performed using one-way ANOVA followed by Dunnett's multiple comparisons test; ****$p < 0.0001$.

GPCR coupling and Gβγ sequestration—have been independently reported for several Gαo variants [21–23]. This apparent contradiction, together with the absence of a unified biosensor approach, prompted us to develop a split-YFP assay to directly visualize the dominant GPCR coupling behavior of Gαo mutants. Using this system, we found that persistent, dominant coupling to activated GPCRs is a common feature among pathogenic Gαo variants. The most severe mutants failed to disengage from activated receptors, thereby blocking GRK-mediated phosphorylation and subsequent endocytosis. In contrast, less severe mutants only partially impaired GPCR phosphorylation without preventing internalization.

BiFC assays have been widely used to analyze protein–protein interactions in living cells [29], including studies on GPCRs, where most applications have focused on receptor homo- and heteromerization [38, 54, 55]. Other BiFC-based approaches have visualized Gβγ dimer formation and localization [56], Src association with GPCRs [38], and β-arrestin recruitment following receptor activation [57, 58]. To our knowledge, this study represents the first BiFC system specifically designed to monitor GPCR coupling by a Gα subunit in mammalian cells. In this assay, YFP complementation at the PM between GPCRs and the Gα appears to be nonselective, as Gαo was able to efficiently tether to the Gs-coupled β_2AR. Upon stimulation,

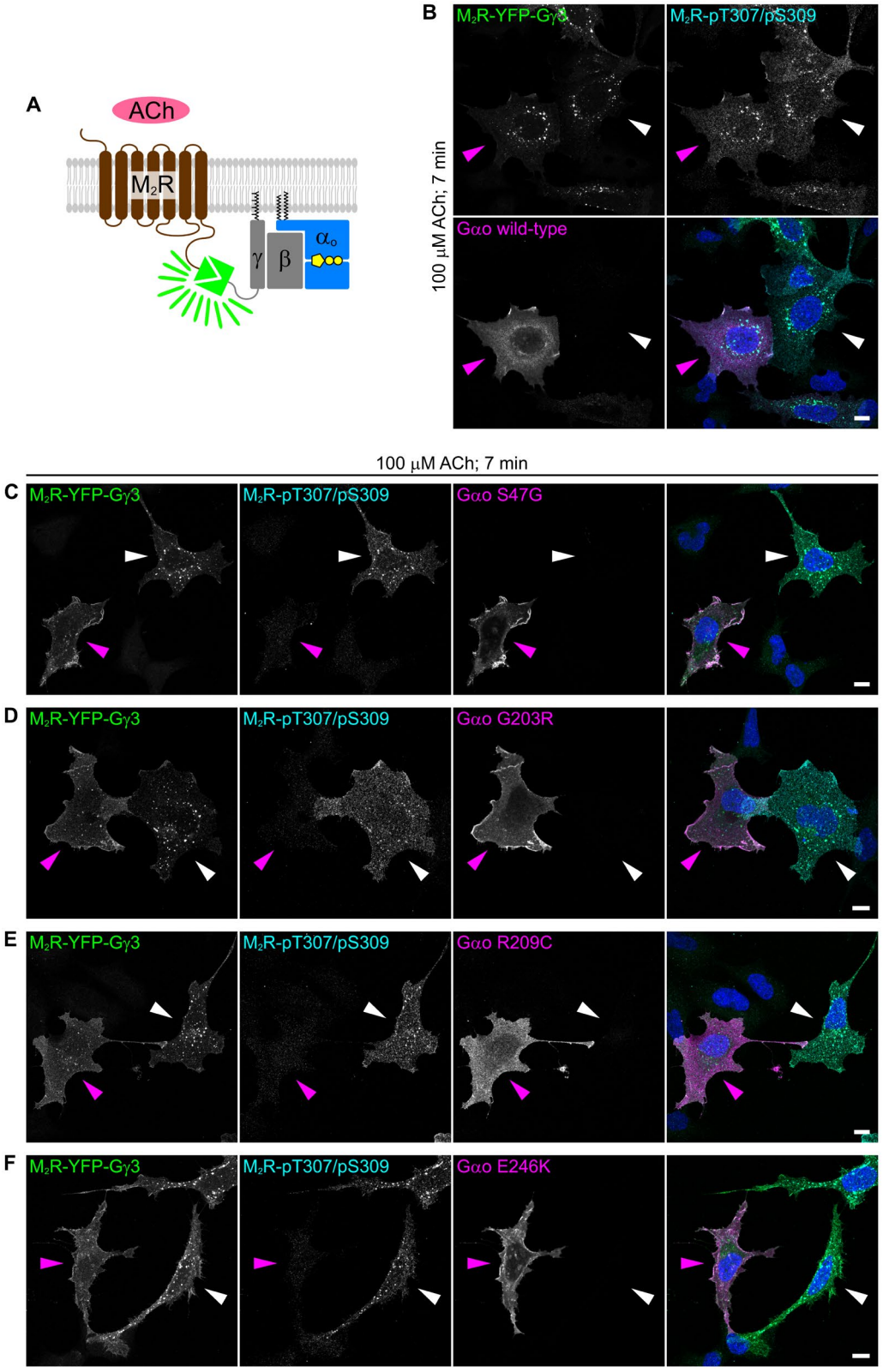

FIGURE 4 | Split-YFP assay with M_2R and Gγ3 recapitulates phosphorylation and endocytosis defects caused by Gαo mutants. (A) Depiction of the split-YFP assay applied to M_2R and Gγ3. (B-F) Confocal images of co-culture of HEK293T cells expressing the M_2R-YFP-Gγ3 complex, with or without co-expression of Gαo wild-type (B), S47G (C), G203R (D), R209C (E), and E246K (F). Cells were stimulated with 100 μM acetylcholine (ACh) for 7 min, then immunostained with anti-pT307/pS309, anti-Gαo, and counterstained with DAPI to visualize nuclei. Magenta and white arrowheads indicate Gαo-expressing and non-expressing cells, respectively. Scale bars, 10 μm.

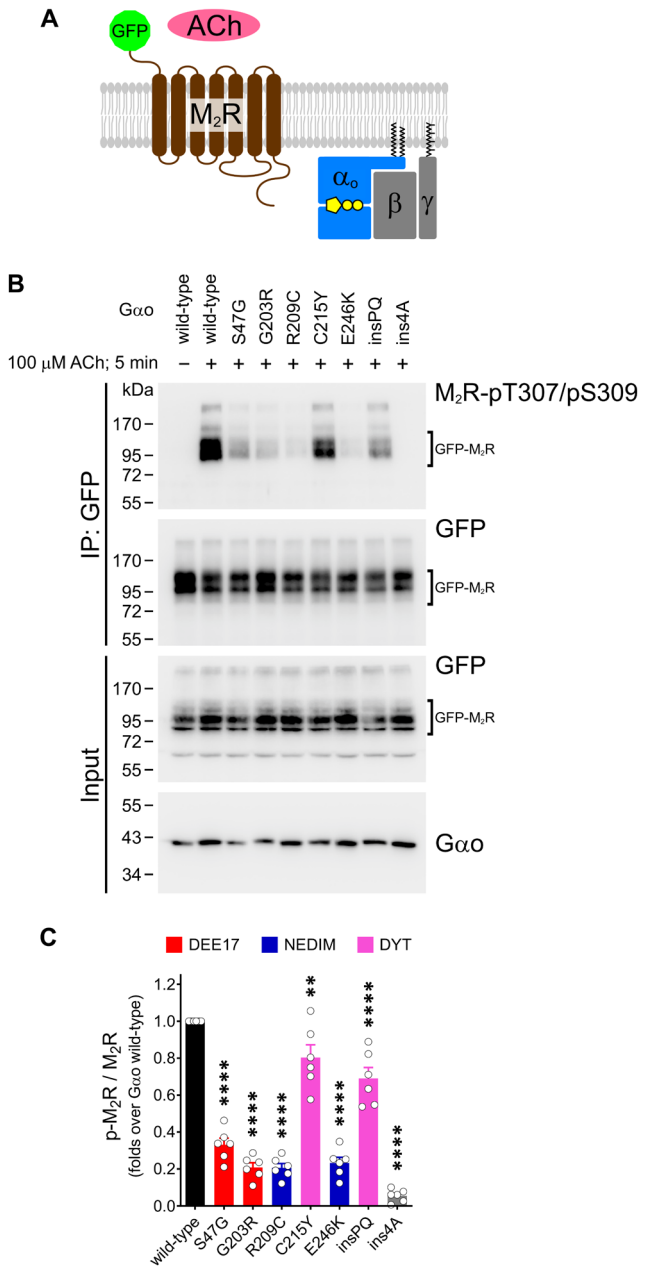

FIGURE 5 | Immunoprecipitation of GFP-M_2R validates dominant GPCR coupling by pathogenic Gαo variants. (A) Diagram of the GFP-M_2R construct and heterotrimeric Gαoβγ, illustrating the lack of intracellular tagging in the proteins. (B) HEK293T cells co-expressing GFP-M_2R and Gαo wild-type, pathogenic mutants, or the ins4A control were stimulated with 100 μM acetylcholine (ACh) for 5 min and subjected to immunoprecipitation (IP) using an anti-GFP nanobody. Western blotting and immunodetection were performed with antibodies against pT307/pS309 and GFP. (C) Quantification of M_2R phosphorylation levels relative to total receptor ($n = 6$). Gαo mutant associations with DEE17, NEDIM, and DYT phenotypes are color-coded. Data represent mean ± SEM. Statistical analysis was performed using one-way ANOVA followed by Dunnett's multiple comparisons test; $^{**}p < 0.005$ and $^{****}p < 0.0001$.

the assay appears highly specific, since pathogenic Gαo variants disrupted internalization of Gi/o-coupled GPCRs but had no effect on β_2AR endocytosis. The irreversibility of the YFP complementation [29] limits the ability of this system to analyze events downstream of G protein activation, as the complemented Gα subunit remains stably associated with the GPCR. This same property, however, allowed us to readily isolate the complemented split-YFP complex using an anti-GFP nanobody [31], enabling biochemical characterization of the GPCR-YFP-Gα complex and potentially opening opportunities for structural studies of dominant GPCR coupling mediated by pathogenic Gαo variants.

In this study, we used HEK293T cells because they allow robust expression of the split-YFP constructs, making the BiFC assay feasible. The non-neuronal nature of this cell line, however, raises the question of whether pathogenic Gαo variants also engage in dominant GPCR coupling under more physiological conditions. Therefore, further studies will be required to confirm this dominant mechanism in neuronal systems, for example using cortical neurons derived from *GNAO1* patient iPSCs as described previously [59].

Dominant GPCR coupling by Gα subunits has long been recognized in the GPCR field [49, 50, 60, 61]. Studies using engineered, non-pathogenic Gα mutations have proposed two mechanistic modes: sequestration of the activated GPCR by the heterotrimeric G protein, or by nucleotide-free Gα subunits. Although our split-YFP assay cannot discriminate between these mechanisms, insight can be drawn from the distinct behaviors of Gαo variants in previous BRET-based assays. For example, the S47G mutant likely traps the receptor—and Gβγ—in an open, intermediate activation state of the heterotrimeric complex, as it was reported to retain near-normal association with Gβγ but shows markedly impaired dissociation upon GPCR activation [21–23]. In contrast, the recurrent G203R, R209C, and E246K variants exhibit significant Gβγ dissociation upon stimulation [21–23, 62], consistent with receptor trapping by nucleotide-free Gαo following Gβγ dissociation (Figure 6). Nevertheless, confirming that these Gαo variants indeed trap activated GPCRs and distinguishing between these two modes will require further mechanistic studies.

In addition to Gαo, dominant GPCR coupling has thus far been implicated only in pathogenic Gαi3 mutations [63]. However, several residues homologous to the Gαo positions analyzed here—Ser47, Gly203, Arg209, and Glu246—are also mutated in other Gα subunits linked to rare genetic conditions [11]: Gαi2 G203R and R209W, Gαolf E255A, Gαs R231C/H and E268K/G, and Gαi3 S47R, which was shown to dominantly couple to the endothelin type A receptor. These observations support the possibility that dominant GPCR coupling may extend beyond Gαo and Gαi3, as many disease-associated mutations affect additional highly conserved residues shared across Gα subunits [11, 12]. Thus, we envision that this simple split-YFP approach could be adapted for routine testing of Gαo and potentially other pathogenic Gα variants implicated in a growing number of rare genetic disorders.

Beyond mechanistic insights, the robustness and scalability of the split-YFP system lay a foundation for drug discovery or repositioning efforts aimed at restoring normal GPCR coupling dynamics. Such applications could accelerate the identification of therapeutic compounds that reverse receptor trapping or

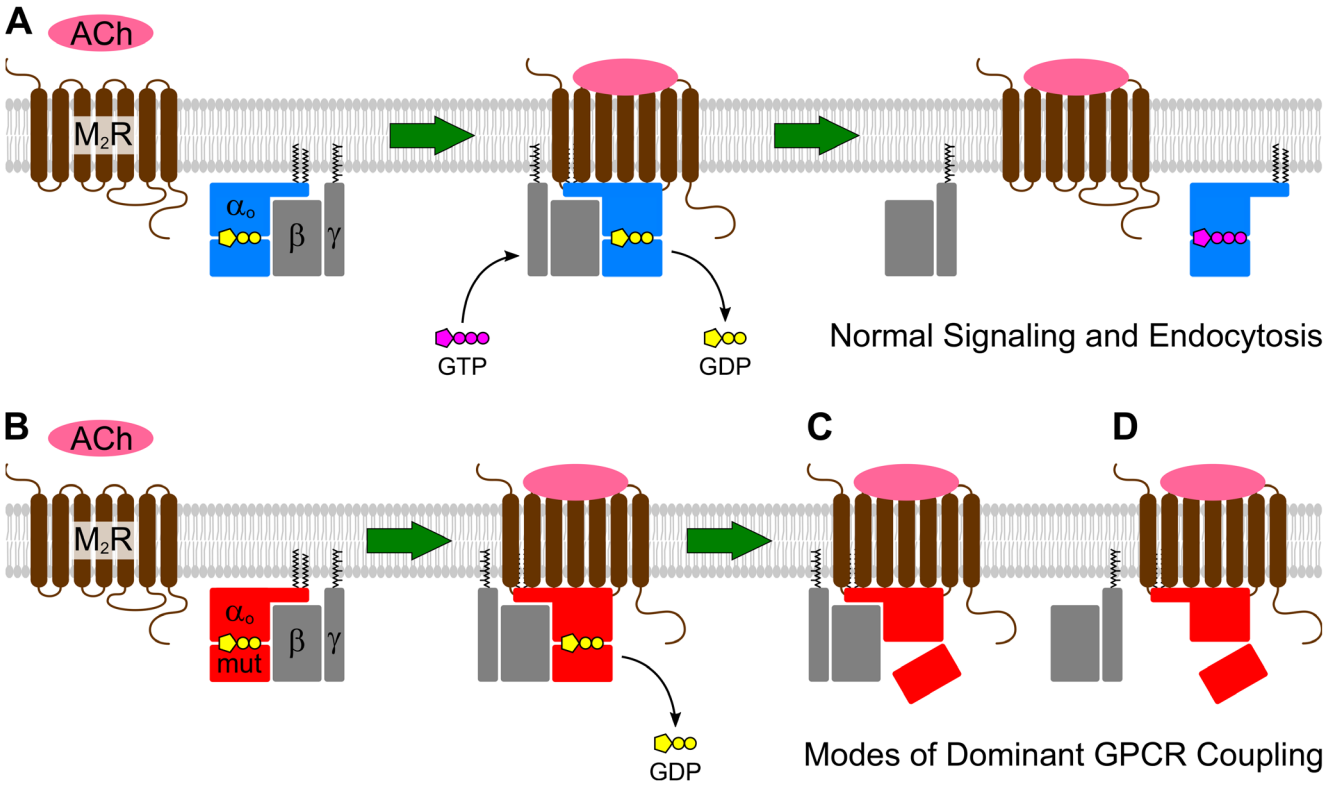

FIGURE 6 | Proposed mechanisms of dominant GPCR coupling by pathogenic Gαo mutants. (A) Under physiological conditions, acetylcholine (ACh) activates the M_2 muscarinic acetylcholine receptor (M_2R), promoting GDP-GTP exchange on wild-type Gαo (blue) within the heterotrimeric G protein. This activation triggers dissociation of Gαo-GTP and Gβγ subunits, initiating downstream signaling and allowing receptor phosphorylation and endocytosis. (B-D) Pathogenic Gαo variants (red) engage activated GPCRs leading to GDP release (B). The failure of Gαo mutants to adopt the active GTP-bound conformation results in dominant GPCR coupling through two distinct mechanisms. In one mode, the mutant Gαo remains in an open, intermediate activation state that retains both the GPCR and Gβγ within a persistent heterotrimeric complex (C). In the second mode, mutant Gαo remains tightly bound to the activated receptor in a nucleotide-free state after Gβγ dissociation (D). Both mechanisms impair receptor phosphorylation and block endocytosis, potentially leading to signaling defects.

promote dissociation of Gαo mutants, offering new avenues for targeted therapies in *GNAO1* encephalopathies.

Author Contributions

Conceptualization: G.P.S. Methodology: C.RdM., G.P.S. Investigation: Y.A.L., G.P.S. Visualization: Y.A.L., G.P.S. Writing-original draft: Y.A.L., G.P.S. Writing-review and editing: M.S., V.L.K., G.P.S. Supervision: V.L.K., G.P.S. All authors reviewed the final manuscript.

Acknowledgments

This study was supported by Famiglie GNAO1 Association grant to G.P.S. We are very thankful to Arthur Radoux-Mergault and Arghavan Kazemzadeh for the valuable discussions and insightful input throughout the development of this project. We thank Sabina Troccaz for her excellent technical assistance. We are grateful to all members of the Bioimaging core facility at the CMU for their expert assistance with microscopy.

Funding

The authors have nothing to report.

Conflicts of Interest

The authors declare no conflicts of interest.

Data Availability Statement

The data that support the findings of this study are available in the Materials and Methods, Results, and Supporting Information of this article.

References

1. T. K. Bjarnadottir, D. E. Gloriam, S. H. Hellstrand, H. Kristiansson, R. Fredriksson, and H. B. Schioth, "Comprehensive Repertoire and Phylogenetic Analysis of the G Protein-Coupled Receptors in Human and Mouse," *Genomics* 88 (2006): 263–273.

2. D. K. Vassilatis, J. G. Hohmann, H. Zeng, et al., "The G Protein-Coupled Receptor Repertoires of Human and Mouse," *Proceedings of the National Academy of Sciences of the United States of America* 100 (2003): 4903–4908.

3. K. L. Pierce, R. T. Premont, and R. J. Lefkowitz, "Seven-Transmembrane Receptors," *Nature Reviews. Molecular Cell Biology* 3 (2002): 639–650.

4. M. J. Marinissen and J. S. Gutkind, "G-Protein-Coupled Receptors and Signaling Networks: Emerging Paradigms," *Trends in Pharmacological Sciences* 22 (2001): 368–376.

5. T. Flock, A. S. Hauser, N. Lund, D. E. Gloriam, S. Balaji, and M. M. Babu, "Selectivity Determinants of GPCR-G-Protein Binding," *Nature* 545 (2017): 317–322.

6. J. Wess, "Molecular Basis of Receptor/G-Protein-Coupling Selectivity," *Pharmacology & Therapeutics* 80 (1998): 231–264.

7. W. M. Oldham and H. E. Hamm, "Heterotrimeric G Protein Activation by G-Protein-Coupled Receptors," *Nature Reviews. Molecular Cell Biology* 9 (2008): 60–71.

8. S. R. Neves, P. T. Ram, and R. Iyengar, "G Protein Pathways," *Science* 296 (2002): 1636–1639.

9. M. B. Dwyer, J. L. Aumiller, and P. B. Wedegaertner, "Going Rogue: Mechanisms, Regulation, and Roles of Mutationally Activated Galpha in Human Cancer," *Molecular Pharmacology* 106 (2024): 198–215.

10. M. O'Hayre, J. Vazquez-Prado, I. Kufareva, et al., "The Emerging Mutational Landscape of G Proteins and G-Protein-Coupled Receptors in Cancer," *Nature Reviews. Cancer* 13 (2013): 412–424.

11. V. L. Katanaev and G. P. Solis, "Dominant Galpha Mutations in Human Disease: Unifying Mechanisms and Treatment Strategies," *EMBO Molecular Medicine* 17 (2025): 2168–2179.

12. L. S. Weinstein, M. Chen, T. Xie, and J. Liu, "Genetic Diseases Associated With Heterotrimeric G Proteins," *Trends in Pharmacological Sciences* 27 (2006): 260–266.

13. L. Briere, M. Thiel, D. A. Sweetser, A. Koy, and E. Axeen, "GNAO1-Related Disorder," in *GeneReviews((R))*, ed. M. P. Adam, S. Bick, G. M. Mirzaa, R. A. Pagon, S. E. Wallace, and A. Amemiya (University of Washington, 1993).

14. V. L. Katanaev, J. Valnohova, D. N. Silachev, Y. A. Larasati, and A. Koval, "Pediatric GNAO1 Encephalopathies: From Molecular Etiology of the Disease to Drug Discovery," *Neural Regeneration Research* 18 (2023): 2188–2189.

15. M. Saez Gonzalez, K. Kloosterhuis, L. van de Pol, F. Baas, and H. Mikkers, "Phenotypic Diversity in GNAO1 Patients: A Comprehensive Overview of Variants and Phenotypes," *Human Mutation* 2023 (2023): 6628283.

16. K. Nakamura, H. Kodera, T. Akita, et al., "De Novo Mutations in GNAO1, Encoding a Galphao Subunit of Heterotrimeric G Proteins, Cause Epileptic Encephalopathy," *American Journal of Human Genetics* 93 (2013): 496–505.

17. L. A. Menke, M. Engelen, M. Alders, V. J. Odekerken, F. Baas, and J. M. Cobben, "Recurrent GNAO1 Mutations Associated With Developmental Delay and a Movement Disorder," *Journal of Child Neurology* 31 (2016): 1598–1601.

18. T. Wirth, G. Garone, M. A. Kurian, et al., "Highlighting the Dystonic Phenotype Related to GNAO1," *Movement Disorders* 37 (2022): 1547–1554.

19. G. P. Solis, Y. A. Larasati, M. Thiel, A. Koval, A. Koy, and V. L. Katanaev, "GNAO1 Mutations Affecting the N-Terminal Alpha-Helix of Galphao Lead to Parkinsonism," *Movement Disorders* 39 (2024): 601–606.

20. G. P. Solis, F. R. Danti, Y. A. Larasati, et al., "Clinical-Molecular Profiling of Atypical GNAO1 Patients: Novel Pathogenic Variants, Unusual Manifestations, and Severe Molecular Dysfunction," *Genes Dis* 12 (2025): 101522.

21. B. S. Muntean, I. Masuho, M. Dao, et al., "Galphao Is a Major Determinant of cAMP Signaling in the Pathophysiology of Movement Disorders," *Cell Reports* 34 (2021): 108718.

22. K. M. Knight, E. G. Obarow, W. Wei, et al., "Molecular Annotation of G Protein Variants in a Neurological Disorder," *Cell Reports* 42 (2023): 113462.

23. G. P. Solis, A. Koval, J. Valnohova, A. Kazemzadeh, M. Savitsky, and V. L. Katanaev, "Neomorphic Galphao Mutations Gain Interaction With Ric8 Proteins in GNAO1 Encephalopathies," *Journal of Clinical Investigation* 134 (2024): e172057.

24. V. L. Katanaev and J. Valnohova, "Molecular Biomarkers in GNAO1 Encephalopathies," *Neural Regeneration Research* 21 (2026): 1570–1571.

25. J. Dominguez-Carral, W. G. Ludlam, M. Junyent Segarra, et al., "Severity of GNAO1-Related Disorder Correlates With Changes in G-Protein Function," *Annals of Neurology* 94 (2023): 987–1004.

26. M. Savitsky, Y. A. Larasati, G. P. Solis, et al., "Loss of the Conserved Switch III Region in a G Protein Leads to Severe Pediatric Encephalopathy," *Science Signaling* 18 (2025): eadu9383.

27. A. Koval, Y. A. Larasati, M. Savitsky, et al., "In-Depth Molecular Profiling of an Intronic GNAO1 Mutant as the Basis for Personalized High-Throughput Drug Screening," *Medicus* 4 (2023): 311–325.

28. K. M. Knight, B. E. Krumm, N. J. Kapolka, et al., "A Neurodevelopmental Disorder Mutation Locks G Proteins in the Transitory Pre-Activated State," *Nature Communications* 15 (2024): 6643.

29. M. G. Romei and S. G. Boxer, "Split Green Fluorescent Proteins: Scope, Limitations, and Outlook," *Annual Review of Biophysics* 48 (2019): 19–44.

30. G. P. Solis, O. Bilousov, A. Koval, A. M. Luchtenborg, C. Lin, and V. L. Katanaev, "Golgi-Resident Galphao Promotes Protrusive Membrane Dynamics," *Cell* 170 (2017): 939–955.

31. G. P. Solis, O. Bilousov, A. Koval, et al., "Pediatric Encephalopathy: Clinical, Biochemical and Cellular Insights Into the Role of Gln52 of GNAO1 and GNAI1 for the Dominant Disease," *Cells* 10 (2021): 2749.

32. E. Malaga-Trillo, G. P. Solis, Y. Schrock, et al., "Regulation of Embryonic Cell Adhesion by the Prion Protein," *PLoS Biology* 7 (2009): e55.

33. M. Stoeber, D. Jullie, B. T. Lobingier, et al., "A Genetically Encoded Biosensor Reveals Location Bias of Opioid Drug Action," *Neuron* 98 (2018): 963–976.

34. H. Schihada, R. Shekhani, and G. Schulte, "Quantitative Assessment of Constitutive G Protein-Coupled Receptor Activity With BRET-Based G Protein Biosensors," *Science Signaling* 14 (2021): eabf1653.

35. G. P. Solis, Y. Schrock, N. Hulsbusch, M. Wiechers, H. Plattner, and C. A. Stuermer, "Reggies/Flotillins Regulate E-Cadherin-Mediated Cell Contact Formation by Affecting EGFR Trafficking," *Molecular Biology of the Cell* 23 (2012): 1812–1825.

36. C. Dong, C. M. Filipeanu, M. T. Duvernay, and G. Wu, "Regulation of G Protein-Coupled Receptor Export Trafficking," *Biochimica et Biophysica Acta* 1768 (2007): 853–870.

37. S. Maeda, Q. Qu, M. J. Robertson, G. Skiniotis, and B. K. Kobilka, "Structures of the M1 and M2 Muscarinic Acetylcholine Receptor/G-Protein Complexes," *Science* 364 (2019): 552–557.

38. M. A. Hauser, K. Schaeuble, I. Kindinger, et al., "Inflammation-Induced CCR7 Oligomers Form Scaffolds to Integrate Distinct Signaling Pathways for Efficient Cell Migration," *Immunity* 44 (2016): 59–72.

39. E. Gottlieb-Abraham, O. Gutman, G. M. Pai, I. Rubio, and Y. I. Henis, "The Residue at Position 5 of the N-Terminal Region of Src and Fyn Modulates Their Myristoylation, Palmitoylation, and Membrane Interactions," *Molecular Biology of the Cell* 27 (2016): 3926–3936.

40. G. P. Solis, A. Kazemzadeh, L. Abrami, et al., "Local and Substrate-Specific S-Palmitoylation Determines Subcellular Localization of Galphao," *Nature Communications* 13 (2022): 2072.

41. J. Kudla and R. Bock, "Lighting the Way to Protein-Protein Interactions: Recommendations on Best Practices for Bimolecular Fluorescence Complementation Analyses," *Plant Cell* 28 (2016): 1002–1008.

42. M. Akgoz, V. Kalyanaraman, and N. Gautam, "Receptor-Mediated Reversible Translocation of the G Protein Betagamma Complex From the Plasma Membrane to the Golgi Complex," *Journal of Biological Chemistry* 279 (2004): 51541–51544.

43. D. Zenko, D. Thompson, and J. N. Hislop, "Endocytic Sorting and Downregulation of the M2 Acetylcholine Receptor Is Regulated by Ubiquitin and the ESCRT Complex," *Neuropharmacology* 162 (2020): 107828.

44. Z. Y. Weinberg and M. A. Puthenveedu, "Regulation of G Protein-Coupled Receptor Signaling by Plasma Membrane Organization and Endocytosis," *Traffic* 20 (2019): 121–129.

45. I. Masuho, R. Kise, P. Gainza, et al., "Rules and Mechanisms Governing G Protein Coupling Selectivity of GPCRs," *Cell Reports* 42 (2023): 113173.

46. A. Radoux-Mergault, L. Oberhauser, S. Aureli, F. L. Gervasio, and M. Stoeber, "Subcellular Location Defines GPCR Signal Transduction," *Science Advances* 9 (2023): eadf6059.

47. J. Duan, H. Liu, F. Zhao, et al., "GPCR Activation and GRK2 Assembly by a Biased Intracellular Agonist," *Nature* 620 (2023): 676–681.

48. R. Ranjan, H. Dwivedi, M. Baidya, M. Kumar, and A. K. Shukla, "Novel Structural Insights Into GPCR-Beta-Arrestin Interaction and Signaling," *Trends in Cell Biology* 27 (2017): 851–862.

49. W. Jang, S. Lu, X. Xu, G. Wu, and N. A. Lambert, "The Role of G Protein Conformation in Receptor-G Protein Selectivity," *Nature Chemical Biology* 19 (2023): 687–694.

50. A. I. Kaya, A. D. Lokits, J. A. Gilbert, T. M. Iverson, J. Meiler, and H. E. Hamm, "A Conserved Hydrophobic Core in Galphai1 Regulates G Protein Activation and Release From Activated Receptor," *Journal of Biological Chemistry* 291 (2016): 19674–19686.

51. R. Pals-Rylaarsdam and M. M. Hosey, "Two Homologous Phosphorylation Domains Differentially Contribute to Desensitization and Internalization of the m2 Muscarinic Acetylcholine Receptor," *Journal of Biological Chemistry* 272 (1997): 14152–14158.

52. B. K. Atwood, J. Lopez, J. Wager-Miller, K. Mackie, and A. Straiker, "Expression of G Protein-Coupled Receptors and Related Proteins in HEK293, AtT20, BV2, and N18 Cell Lines as Revealed by Microarray Analysis," *BMC Genomics* 12 (2011): 14.

53. S. Marsango, R. J. Ward, E. Alvarez-Curto, and G. Milligan, "Muscarinic Receptor Oligomerization," *Neuropharmacology* 136 (2018): 401–410.

54. K. F. Ejendal, J. M. Conley, C. D. Hu, and V. J. Watts, "Bimolecular Fluorescence Complementation Analysis of G Protein-Coupled Receptor Dimerization in Living Cells," *Methods in Enzymology* 521 (2013): 259–279.

55. J. Liang, M. Seghiri, P. K. Singh, et al., "The beta2-Adrenergic Receptor Associates With CXCR4 Multimers in Human Cancer Cells," *Proceedings of the National Academy of Sciences of the United States of America* 121 (2024): 897121.

56. T. R. Hynes, E. A. Yost, S. M. Yost, and C. H. Berlot, "Multicolor BiFC Analysis of G Protein Betagamma Complex Formation and Localization," *Methods in Molecular Biology* 756 (2011): 229–243.

57. L. E. Kilpatrick, S. J. Briddon, S. J. Hill, and N. D. Holliday, "Quantitative Analysis of Neuropeptide Y Receptor Association With Beta-arrestin2 Measured by Bimolecular Fluorescence Complementation," *British Journal of Pharmacology* 160 (2010): 892–906.

58. Y. B. Song, C. O. Park, J. Y. Jeong, and W. K. Huh, "Monitoring G Protein-Coupled Receptor Activation Using an Adenovirus-Based Beta-Arrestin Bimolecular Fluorescence Complementation Assay," *Analytical Biochemistry* 449 (2014): 32–41.

59. M. C. Benedetti, T. D'Andrea, A. Colantoni, et al., "Cortical Neurons Obtained From Patient-Derived iPSCs With GNAO1 p.G203R Variant Show Altered Differentiation and Functional Properties," *Heliyon* 10 (2024): e26656.

60. S. Ramachandran and R. A. Cerione, "A Dominant-Negative Galpha Mutant That Traps a Stable Rhodopsin-Galpha-GTP-Betagamma Complex," *Journal of Biological Chemistry* 286 (2011): 12702–12711.

61. Y. L. Liang, P. Zhao, C. Draper-Joyce, et al., "Dominant Negative G Proteins Enhance Formation and Purification of Agonist-GPCR-G Protein Complexes for Structure Determination," *ACS Pharmacology & Translational Science* 1 (2018): 12–20.

62. Y. A. Larasati, M. Savitsky, A. Koval, G. P. Solis, J. Valnohova, and V. L. Katanaev, "Restoration of the GTPase Activity and Cellular Interactions of Galpha(o) Mutants by Zn(2+) in GNAO1 Encephalopathy Models," *Science Advances* 8 (2022): eabn9350.

63. A. Marivin, A. Leyme, K. Parag-Sharma, et al., "Dominant-Negative Galpha Subunits Are a Mechanism of Dysregulated Heterotrimeric G Protein Signaling in Human Disease," *Science Signaling* 9 (2016): ra37.

Supporting Information

Additional supporting information can be found online in the Supporting Information section. **Data S1:** Supplementary Figures.